Probing the $WW\gamma$ vertex at the Fermilab Tevatron Collider

U. Baur*
CERN, Geneva, Switzerland

E. L. Berger
High Energy Physics Division, Argonne National Laboratory, Argonne, Illinois 60439
(Received 25 September 1989)

A detailed analysis of $W\gamma$ production and radiative W decays at the Fermilab Tevatron is presented for general $WW\gamma$ couplings. Possibilities to test the gauge structure of the $WW\gamma$ vertex are explored. At the Tevatron, for an integrated luminosity of 100 pb^{-1}, the $WW\gamma$ vertex can be measured with 25–40 % accuracy in $W\gamma$ production. The limits which can be obtained from radiative W decays are found to be significantly weaker.

I. INTRODUCTION

The Collider Detector at Fermilab (CDF) Collaboration collected data corresponding to an integrated luminosity of about 4.7 pb^{-1} during the last run of the Fermilab Tevatron $p\bar{p}$ collider,[1] operating at $\sqrt{s}=1.8$ TeV. The inclusive cross sections of W- and Z-boson production are about 21 and 6 nb at the Tevatron. Thus a large sample of weak bosons has been obtained which makes it possible to study the properties of W and Z production in $p\bar{p}$ collisions in detail. In particular the production of weak bosons associated with one or more hadronic jets will provide further tests of perturbative QCD at energies beyond the reach of the CERN $p\bar{p}$ collider. In future runs an integrated luminosity of up to 100 pb^{-1} can be expected.[2] It will then be possible to investigate also electroweak corrections to weak-boson production, such as radiative W decays, $W\to f\bar{f}'\gamma$, and $W\gamma$ production. If the W decay into a fermion-antifermion pair $f\bar{f}'$ is included in $p\bar{p}\to W\gamma$, both processes result in the same final state.

$W\gamma$ production and radiative W decays are particularly interesting theoretically since they depend on the $WW\gamma$ coupling which, so far, has not been tested experimentally. Within the standard model (SM), at the tree level, the $WW\gamma$ vertex is completely fixed by the gauge theory structure of the model. The observation of the $WW\gamma$ coupling thus is a crucial test of the SM.

In this paper we study the capability of future experiments at the Tevatron to probe the $WW\gamma$ vertex via $W\gamma$ production and radiative W decays. In the past many authors have considered these processes[3–9] usually with emphasis on the anomalous magnetic moment of the W as a non-gauge-theory contribution. In our analysis we go a step further and use the most general $WW\gamma$ coupling which is accessible in the annihilation processes $q\bar{q}'\to W\gamma$ and $q\bar{q}'\to W\to f\bar{f}'\gamma$ of effectively massless quarks. Four different anomalous couplings are allowed by electromagnetic gauge invariance and Lorentz invariance,[10,11] and their properties are discussed in Sec. II. Apart from anomalies in the $WW\gamma$ vertex we assume the SM to be valid. In particular we assume the coupling of W and Z bosons to quarks and leptons to be given by the SM.

Our analysis is based on the calculation of helicity amplitudes for the complete processes

$$q\bar{q}'\to W^{\pm}\gamma,\quad W^{\pm}\to e^{\pm}\nu \tag{1.1}$$

and

$$q\bar{q}'\to W^{\pm}\to e^{\pm}\nu\gamma\ . \tag{1.2}$$

If finite-W-width effects are included, both reactions are described by the same gauge-invariant set of Feynman diagrams and, in principle, radiative W decays and $W\gamma$ production can no longer be distinguished. By imposing suitable kinematic cuts it is possible, however, to isolate regions in phase space where the major part of the cross section results from radiative W decays, or from W-photon production. These cuts are described in detail in Sec. III, which also contains a brief discussion of the QCD corrections[12] to (1.1) and (1.2) and the background from W-jet production, with the jet misidentified as a photon. In Sec. IV we discuss the signatures for anomalous $WW\gamma$ couplings. Constraints on anomalous contributions to the $WW\gamma$ vertex exist already, derived either from low-energy experiments[13–20] or from unitarity considerations.[14,21] To avoid confusion we shall first discuss the expected signals in (1.1) and (1.2) without taking into account the low-energy bounds. In Sec. V we then compare the sensitivity to anomalous $WW\gamma$ couplings expected at the Tevatron with the low-energy bounds and with the sensitivity expected from $ep\to eW^{\pm}X$ at DESY HERA and $e^+e^-\to W^+W^-$ at CERN LEP 200. We comment on limits which can be obtained with the present data samples from CDF and the CERN UA2 experiment. In Sec. V we also present our conclusions.

II. THE $WW\gamma$ VERTEX

At the parton level, if finite-W-width effects are ignored, the reaction $p\bar{p}\to W^{\pm}\gamma$ proceeds via the Feynman graphs shown in Fig. 1(a)–1(c). The diagrams of Fig. 1(c)–1(e) describe radiative W decays. The $WW\gamma$ vertex in which we are interested enters via diagram 1(c). In

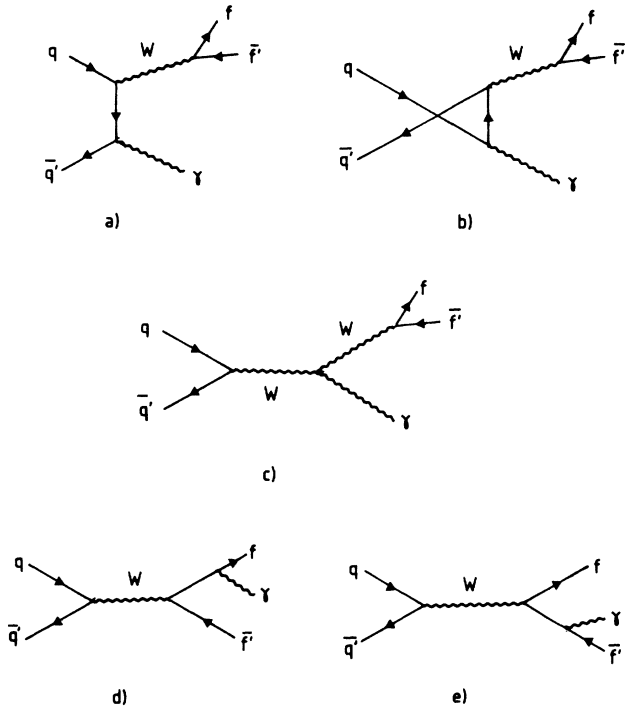

FIG. 1. Feynman graphs for the parton-level processes contributing to $p\bar{p}\to W\gamma$, $W\to f\bar{f}'$, and $p\bar{p}\to W\to f\bar{f}'\gamma$. If finite-$W$-width effects are taken into account, all diagrams have to be included in the calculation in order to preserve electromagnetic gauge invariance.

both processes the virtual and the on-shell W both couple to essentially massless fermions, which ensures that effectively $\partial_\mu W^\mu=0$. This together with gauge invariance of the on-shell photon restricts the tensor structure of the WW photon vertex sufficiently to allow just four free parameters, which are conveniently described by the effective Lagrangian[10,11,22]

$$\mathcal{L}_{WW\gamma}=-ie\left\{(W^\dagger_{\mu\nu}W^\mu A^\nu-W^\dagger_\mu A_\nu W^{\mu\nu})+\kappa W^\dagger_\mu W_\nu F^{\mu\nu}+\frac{\lambda}{M_W^2}W^\dagger_{\lambda\mu}W^\mu_\nu F^{\nu\lambda}+\tilde{\kappa}W^\dagger_\mu W_\nu \tilde{F}^{\mu\nu}+\frac{\tilde{\lambda}}{M_W^2}W^\dagger_{\lambda\mu}W^\mu_\nu \tilde{F}^{\nu\lambda}\right\} . \quad (2.1)$$

Here A^μ and W^μ are the photon and W^- fields, respectively, $W_{\mu\nu}=\partial_\mu W_\nu-\partial_\nu W_\mu$, $F_{\mu\nu}=\partial_\mu A_\nu-\partial_\nu A_\mu$, and $\tilde{F}_{\mu\nu}=\frac{1}{2}\epsilon_{\mu\nu\rho\sigma}F^{\rho\sigma}$. e is the charge of the proton, and M_W represents the W-boson mass.

The first term in Eq. (2.1) arises from minimal coupling of the photon to the $W^\pm$ fields and is completely fixed by the charge of the W boson for on-shell photons. While the κ and λ terms do not violate any discrete symmetries, the $\tilde{\kappa}$ and $\tilde{\lambda}$ terms are P odd and CP violating. Within the SM, at the tree level,

$$\kappa=1,\quad \lambda=0,\quad \tilde{\kappa}=0,\quad \tilde{\lambda}=0 . \quad (2.2)$$

The κ ($\tilde{\kappa}$) and λ ($\tilde{\lambda}$) terms are related to the magnetic (electric) dipole moment μ_W (d_W) and the electric (magnetic) quadrupole moment Q_W ($\tilde{Q}_W$) of the W^+:

$$\mu_W=\frac{e}{2M_W}(1+\kappa+\lambda) , \quad (2.3a)$$

$$Q_W=-\frac{e}{M_W^2}(\kappa-\lambda) , \quad (2.3b)$$

$$d_W=\frac{e}{2M_W}(\tilde{\kappa}+\tilde{\lambda}) , \quad (2.3c)$$

$$\tilde{Q}_W=-\frac{e}{M_W^2}(\tilde{\kappa}-\tilde{\lambda}) . \quad (2.3d)$$

Tree-level unitarity, e.g., for the process $e^+e^-\to W^+W^-$, uniquely restricts the $WW\gamma$ couplings to their (SM) gauge-theory values at asymptotically high energies.[23] This implies that any deviation $a=\kappa-1,\ldots,\tilde{\lambda}$ from the SM expectation has to be described by a form factor $a(q^2,\bar{q}^2,q_\gamma^2)$ which vanishes when one of the arguments, the square of the four-momentum of one of the W bosons, q^2 or $\bar{q}^2$, or the square of the four-momentum of the photon, q_γ^2, becomes large. For deviations of the three vector-boson couplings from the gauge theory value, produced by some novel interactions operative at a scale Λ, one should expect that the form factors stay essentially constant for center-of-mass energies $\sqrt{\hat{s}}<\Lambda$ and start decreasing only when the scale Λ is reached or surpassed, very much like the well-known nucleon form factors. Present experimental data suggest that Λ is at least of the order of a few hundred GeV (Ref. 24). Since the energy region covered by the Tevatron is smaller than typically expected for Λ we may assume the form factors $a=\kappa-1,\ldots,\tilde{\lambda}$ to be approximately constant in the following.

The effective Lagrangian (2.1) leads to cross-section formulas for the processes (1.1) and (1.2), including the effect of anomalous $WW\gamma$ couplings. When the decay of the W into a massless fermion antifermion pair $f\bar{f}'$ and a finite-width W propagator are taken into account, all the Feynman graphs of Fig. 1 have to be included in the calculation of each process in order to preserve electromagnetic gauge invariance. $W\gamma$ production and radiative W decays then result in the same final state and are described by the same set of diagrams. As a result the two processes interfere and, in principle, can no longer be distinguished. For our numerical simulations we have calculated the complete matrix elements corresponding to the diagrams of Fig. 1 by making use of the helicity techniques described in Ref. 25.

Since anomalous $WW\gamma$ couplings influence different quantities in the two processes, it is necessary to isolate those regions in phase space where the dominant part of the cross section results from radiative W decays and $W\gamma$ production, respectively. As we shall see in the next section this can be achieved rather easily so that in practice it is legitimate to distinguish $p\bar{p}\to W\gamma$, $W\to f\bar{f}'$ from $p\bar{p}\to W\to f\bar{f}'\gamma$.

For our later phenomenological discussion we find it convenient to display the contributions of anomalous

couplings to the $q\bar{q}' \to W\gamma$ helicity amplitudes, neglecting the W decay. The helicity of the incoming, effectively massless, quark (antiquark) is fixed to be $-\frac{1}{2}(+\frac{1}{2})$ by the $V-A$ structure of the $Wq\bar{q}'$ coupling. This means that the anomalous contributions to the $W\gamma$ production amplitudes depend only on the W and photon helicities, λ_W and λ_γ. Denoting these contributions by $\Delta\mathcal{M}_{\lambda_\gamma\lambda_W}$, one finds

$$\Delta\mathcal{M}_{\pm 0}=\frac{e^2}{\sin\theta_W}\frac{\sqrt{\hat{s}}}{2M_W}[\kappa-1+\lambda\mp i(\tilde{\kappa}+\tilde{\lambda})]\tfrac{1}{2}(1\mp\cos\Theta)\,,$$
$$\Delta\mathcal{M}_{\pm\pm}=\frac{e^2}{\sin\theta_W}\frac{1}{2}\left[\frac{\hat{s}}{M_W^2}(\lambda\mp i\tilde{\lambda})+(\kappa-1\mp i\tilde{\kappa})\right]\frac{1}{\sqrt{2}}\sin\Theta\,, \tag{2.4}$$

where Θ denotes the scattering angle of the photon with respect to the quark direction, measured in the $W\gamma$ rest frame, and $\sqrt{\hat{s}}$ is the invariant mass of the W-photon system.

Since the structure of the $WW\gamma$ vertex enters (1.1) and (1.2) via the s-channel exchange of a W boson [see Fig. 1(c)], only the four helicity combinations in Eq. (2.4) are affected by anomalous couplings. The helicity combinations $(\lambda_\gamma,\lambda_W)=(+-)$ and $(-+)$ have the photon and W spins aligned along the photon momentum direction and hence have angular momentum $J\geq 2$: they cannot be reached by s-channel exchange of a vector boson. The fact that only the above four helicity combinations of the $J=1$ partial wave can be reached by s-channel W exchange explains why four free parameters suffice to parametrize the effects of the most general $WW\gamma$ vertex in $W\gamma$ production.

A pronounced feature of $W\gamma$ production in $q\bar{q}'$ annihilation is the SM prediction of radiation zeros in all contributing helicity amplitudes at one value of the photon scattering angle Θ and hence in the differential cross section.[4] For $u\bar{d}\to W^+\gamma$ this radiation zero occurs at $\cos\Theta=-\frac{1}{3}$. In the presence of any anomalous contribution to the $WW\gamma$ vertex the radiation zero will be at least partially eliminated. This is obvious from Eq. (2.4): none of the anomalous contributions to the scattering amplitudes vanishes at $\cos\Theta=-\frac{1}{3}$.

While the SM contribution to the $q\bar{q}'\to W\gamma$ scattering amplitudes is bounded for fixed scattering angle Θ, the anomalous contributions (2.4) rise without limit as $\hat{s}$ increases, eventually violating unitarity. This is the reason the anomalous couplings must show a form-factor behavior at very high energies. Anomalous values of λ or $\tilde{\lambda}$ are enhanced by $\hat{s}/M_W^2$ in the amplitudes $\mathcal{M}_{\pm\pm}$, whereas terms containing κ and $\tilde{\kappa}$ mainly contribute to $\mathcal{M}_{\pm 0}$ and grow only with $\sqrt{\hat{s}}/M_W$. For large values of the $W\gamma$ invariant mass $\sqrt{\hat{s}}$, the amplitudes (2.4) will dominate the SM contributions and suffice to explain differential distributions of the photon and the W decay products.

In contrast with $W\gamma$ production, the available center-of-mass energy $\sqrt{\hat{s}}$ is fixed to $\sqrt{\hat{s}}\approx M_W$ in radiative W decays. Hence, the anomalous contributions to the $q\bar{q}'\to W\to f\bar{f}'\gamma$ helicity amplitudes do not dominate the SM amplitudes, unless very large values are chosen for the anomalous couplings. The sensitivity of radiative W decays to anomalous $WW\gamma$ couplings results mostly from a radiation zero which, in the SM, is present in the angular distribution of the photon in the W rest frame.[4] Similar to the situation in W-photon production, the radiation zero disappears for any nonzero anomalous coupling.

III. SIGNAL AND EXPERIMENTAL CUTS

As we have seen, W-photon production and radiative W decays both lead to the same final state consisting of a fermion-antifermion pair and a photon when the W decay in $p\bar{p}\to W\gamma$ is taken into account. The hadronic decay modes of the W will be difficult to observe due to the QCD $jj\gamma$ background.[26] If only leptonic decay modes are considered, about 20% of all W decays are still observable (we neglect the $W\to\tau\nu$ decay in the following).

To be more specific, we shall focus in our work on final states which contain either an electron or a positron. The signal we consider is

$$p\bar{p}\to e^{\pm}+\gamma+\not{p}_T\,, \tag{3.1}$$

with the missing transverse momentum $\not{p}_T$ resulting from the nonobservation of the neutrino arising either from the $W\to e\nu$ or the $W\to e\nu\gamma$ decay. We include the leptonic branching fraction

$$B=B(W\to e\nu)=0.109 \tag{3.2}$$

corresponding to a top-quark mass $m_t>M_W$ in all subsequent figures. For $e\gamma\not{p}_T$ events originating from $W\gamma$ production, the electron and the photon are expected to be well isolated, whereas for events resulting from $W\to e\nu\gamma$ the photon tends to be collinear with the charged lepton. This point will be discussed in more detail at the end of this section.

A serious background to the signal (3.1) may be caused by W jet production with the jet misidentified as a photon. Such misidentifications originate mostly from jets hadronizing with a leading π^0, which carries away most of the jet energy. In the CDF detector the photons arising from the π^0 decay usually can be separated if the transverse momentum p_T of the π^0 is smaller than about 50 GeV (Ref. 27). Thus, the W jet background is not expected to pose problems in the region $p_{T\gamma}<50$ GeV.

For photon transverse momenta $p_{T\gamma}>50$ GeV the W jet background cannot be neglected. A precise value for the probability $P_{\gamma/j}$ that a jet of $p_T>50$ GeV is misidentified as a single photon depends on details of the jet structure. Since π^0's and photons have rather different shower profiles in an electromagnetic calorimeter $P_{\gamma/j}$ will be small. In a preliminary study,[28] values of $P_{\gamma/j}=(2-5)\times 10^{-3}$ were found for $p_{T\gamma}>10$ GeV at Tevatron energies. Because $P_{\gamma/j}$ becomes rapidly smaller with increasing $p_{T\gamma}$ (Ref. 29), one expects that the misidentification probability for $p_{T\gamma}>50$ GeV will be significantly smaller than 5×10^{-3}. In Sec. IV we shall study in more detail the impact of the W jet background on the sensitivity of (3.1) to anomalies in the $WW\gamma$ vertex.

Another source of backgrounds may be other standard-model physics processes which produce leptons in association with hard photons and missing transverse momentum. One candidate is prompt photon production in association with a charm or bottom quark, produced by the QCD subprocess $Qg \to Q\gamma$. Semileptonic decay of the heavy quark Q will yield the required lepton and missing transverse momentum. We have not made a detailed study of this and other possibilities, but we note that the decay of a bottom or charm quark does not yield an isolated lepton. A lepton close to a hadronic jet is unlikely to be confused with a lepton originating from W decay.

For our analysis of signatures of anomalous $WW\gamma$ couplings it is important to distinguish $W\gamma$ production efficiently from radiative W decays. In radiative W decays the $e^{\pm}\nu$ pair and the photon form a system with invariant mass $M(e\nu\gamma)$ close to M_W. For $W\gamma$ production, on the other hand, $M(e\nu\gamma)$ is always larger than M_W if finite-W-width effects are ignored. This difference suggests that $e^{\pm}\gamma\not{p}_T$ events originating from radiative W decays can be separated by a $M(e\nu\gamma)$ cut from $W\gamma$ events which result in the same final state. However, because of the nonobservation of the neutrino, $M(e\nu\gamma)$ cannot be determined unambigously and the minimum invariant mass or the cluster transverse mass[30] is more useful:

$$M_T^2(e\gamma;\not{p}_T)=[(M_{e\gamma}^2+|\mathbf{p}_{T\gamma}+\mathbf{p}_{Te}|^2)^{1/2}+\not{p}_T]^2 - |\mathbf{p}_{T\gamma}+\mathbf{p}_{Te}+\not{\mathbf{p}}_T|^2 , \tag{3.3}$$

where $M_{e\gamma}$ denotes the invariant mass of the $e\gamma$ pair. For $W\to e\nu\gamma$ the cluster transverse mass sharply peaks at M_W (Ref. 30) and drops rapidly above the W mass. Thus $e\gamma\not{p}_T$ events originating from $W\gamma$ production and radiative W decays can be distinguished if $M_T(e\gamma;\not{p}_T)$ is cut slightly above M_W (Ref. 8). In the following we shall identify events which satisfy

$$M_T(e\gamma;\not{p}_T)<90 \text{ GeV} \tag{3.4a}$$

with radiative W decays whereas $W\gamma$ events are selected by

$$M_T(e\gamma;\not{p}_T)>90 \text{ GeV} . \tag{3.4b}$$

We shall see below that the M_T cut is quite efficient in distinguishing the two processes.

Effects of higher-order QCD corrections are simulated for both radiative W decays and $W\gamma$ production by a K factor

$$K=1+\tfrac{8}{9}\pi\alpha_s(\hat{s}) , \tag{3.5}$$

where α_s is the strong coupling constant. In the narrow-W-width approximation QCD corrections to $q\bar{q}' \to W\to e\nu\gamma$ are identical to the QCD corrections for single W production in $p\bar{p}$ collisions and can well be approximated by a K factor. Recently the full $O(\alpha_s)$ QCD corrections to $W\gamma$ production have been computed.[12,31] It turns out that, for Tevatron energies, the QCD corrections to $q\bar{q}'\to W\gamma$ also can be represented quite well by a K factor. The radiation zero is affected insignificantly by the QCD corrections. By approximating QCD corrections by a K-factor one, however, ignores the transverse momentum of the produced W or $W\gamma$ system induced by the higher-order terms.

Finite detector acceptance is simulated by cuts imposed on the final-state particles. In the following we require a photon transverse momentum of $p_{T\gamma}>10$ GeV, an electron photon separation in the pseudorapidity–azimuthal-angle plane

$$\Delta R_{e\gamma}=[(\Delta\phi_{e\gamma})^2+(\Delta\eta_{e\gamma})^2]^{1/2}>0.7 , \tag{3.6}$$

and a missing p_T of $\not{p}_T>20$ GeV. Uncertainties in the energy measurements of the $e^{\pm}$ and the photon in the detector are taken into account by Gaussian smearing of the particle four-momenta with standard deviation $\sigma=(0.15 \text{ GeV}^{1/2})\sqrt{E}$. In fact, without a finite $p_{T\gamma}$ and $\Delta R_{e\gamma}$ cut the cross section for (3.1) would diverge, due to the various collinear and infrared singularities which are present. The $\not{p}_T$ cut, on the other hand, has only a small effect on the cross section because the missing-transverse-momentum distribution shows the familiar Jacobian peak at $p_T\approx\frac{1}{2}M_W$ for both $W\gamma$ production and the radiative W decay.

Electrons can be identified by the CDF detector in the pseudorapidity range $|\eta_e|\lesssim 2$, but their charge can only be determined in the central region $|\eta_e|<1.1$. The minimum electron p_T required in the CDF detector depends somewhat on η_e. For $|\eta_e|<1.1$ a minimum transverse momentum of $p_{T_e}>15$ GeV is sufficient while for $|\eta_e|>1.1$ a slightly higher threshold of ≈ 20 GeV is required.[32]

Figure 2 shows the electron transverse-momentum spectrum for $p\bar{p}\to W^{\pm}\gamma$; $W^{\pm}\to e^{\pm}\nu$ (solid line) and $p\bar{p}\to W^{\pm}\to e^{\pm}\nu\gamma$ (dashed line). For $q\bar{q}'\to W\gamma$; $W\to e\nu$ the p_{Te} distribution exhibits the familiar Jacobian peak at $p_{Te}\approx\frac{1}{2}M_W\approx 40$ GeV, smeared by the W's transverse momentum. It is obvious that a transverse-momentum cut of ≤ 30 GeV has almost no effect on the $W\gamma$ cross section. In the following we shall impose a pseudorapidity cut of $|\eta_e|<2$ and an electron p_T cut of $p_{Te}>20$ GeV in $p\bar{p}\to W\gamma$, $W\to e\nu$. Since the electron charge cannot be measured for $|\eta_e|>1.1$ we shall sum over the W charges. Restriction to the central pseudorapidity region ($|\eta_e|<1.1$) would result in only half the rate for $|\eta_e|<2$ in the phase-space region which is sensitive to anomalous $WW\gamma$ couplings.

The SM parameters used in Fig. 2 and all subsequent figures are $\alpha=\alpha(M_W)=\frac{1}{128}$, $M_W=82$ GeV, and $\sin^2\theta_W=0.23$. Our results remain unchanged if M_W is varied by a few GeV. For the parton distribution functions we use set 1 of Duke and Owens[33] with the scale Q^2 given by the parton center-of-mass energy squared, $\hat{s}$.

In contrast with $W\gamma$ production the $p\bar{p}\to W^{\pm}\to e^{\pm}\nu\gamma$ cross section is quite sensitive to the p_{Te} threshold. The electron transverse-momentum spectrum for this process is rather flat up to $p_{Te}\approx 30$ GeV and drops sharply above this value (see Fig. 2). Because of the higher p_{Te} threshold in the region $|\eta_e|>1.1$, the major part ($\approx 85\%$) of the visible $p\bar{p}\to W\to e\nu\gamma$ cross section arises from the

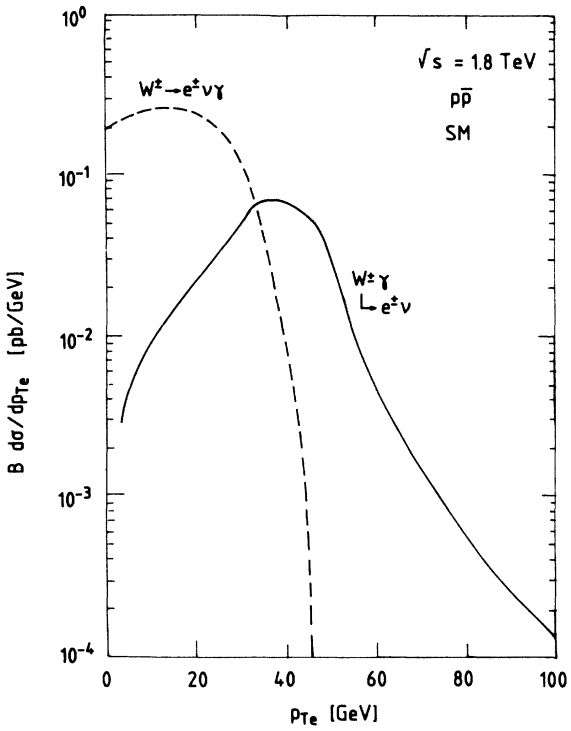

FIG. 2. Transverse-momentum spectrum of the $e^{\pm}$ arising in $p\bar{p}\to W^{\pm}\gamma$, $W^{\pm}\to e^{\pm}\nu$ [solid line; $M_T(e\gamma;\not{p}_T)>90$ GeV] and $p\bar{p}\to W^{\pm}\to e^{\pm}\nu\gamma$ [dashed line; $M_T(e\gamma;\not{p}T)<90$ GeV] at $\sqrt{s}=1.8$ TeV in the SM. The p_T cuts of $p_{T\gamma}>10$ GeV and $\not{p}_T>20$ GeV, and an electron-photon isolation cut of $\Delta R_{e\gamma}>0.7$ are imposed. QCD corrections are simulated by a K factor.

central pseudorapidity region $|\eta_e|<1.1$. We therefore impose a $p_{Te}>15$ GeV cut and restrict η_e to $|\eta_e|<1.1$ for radiative W decays.

The CDF detector can detect photons with good efficiency if their pseudorapidity is $|\eta_\gamma|<1$. In events where one does not trigger on photons this region can be enlarged, perhaps to $|\eta_\gamma|<3$. As we shall see in Sec. IV, anomalous $WW\gamma$ couplings affect mainly the small photon pseudorapidity region. In the following we thus require that $|\eta_\gamma|<1$. Our cuts can then be summarized as follows:

$p\bar{p}\to W\gamma,\ W\to e\nu$	$p\bar{p}\to W\to e\nu\gamma$
$M_T(e\gamma;\not{p}_T)>90$ GeV	$M_T(e\gamma;\not{p}_T)<90$ GeV
$p_{T\gamma}>10$ GeV	$p_{T\gamma}>10$ GeV
$\lvert\eta_\gamma\rvert<1$	$\lvert\eta_\gamma\rvert<1$
$\Delta R_{e\gamma}>0.7$	$\Delta R_{e\gamma}>0.7$
$\not{p}_T>20$ GeV	$\not{p}_T>20$ GeV
$p_{Te}>20$ GeV	$p_{Te}>15$ GeV
$\lvert\eta_e\rvert<2$	$\lvert\eta_e\rvert<1.1$

(3.7)

For our subsequent analysis of signatures of anomalous $WW\gamma$ couplings it is important to know how well the cluster transverse mass cuts actually separate radiative W decays from $W\gamma$ production when all other cuts of (3.7) are taken into account. The normalized distribution of the electron-photon separation $(1/\sigma)(d\sigma/d\Delta R_{e\gamma})$, which is shown in Fig. 3, provides a good test for the efficiency of (3.4a) and (3.4b). The $M_T(e\gamma;\not{p}_T)$ cut of 90 GeV is efficient in removing the $W\gamma$ background for $M_T(e\gamma;\not{p}_T)<90$ GeV and the $W\to e\nu\gamma$ background for $M_T(e\gamma;\not{p}_T)>90$ GeV. For radiative W decays (dashed line) the $\Delta R_{e\gamma}$ distribution exhibits a strong peaking at small separations due to the collinear bremsstrahlung singularities in the cross section, and it falls off very rapidly for large values of $\Delta R_{e\gamma}$. In $W\gamma$ production, in the SM, the electron tends to be emitted in the direction of the parent W (Ref. 11). Thus the electron and the photon should be essentially back to back, implying a peak near $\Delta R_{e\gamma}=\pi$. This peak is clearly visible in Fig. 3 (solid line). We also observe that no visible trace is left of the collinear singularity at small $\Delta R_{e\gamma}$ values, indicating that the contributions from $W\to e\nu\gamma$ for $M_T(e\gamma;\not{p}_T)>90$ GeV are small.

From Fig. 3 it is evident that the $\Delta R_{e\gamma}$ cut has almost no effect on the $W\gamma$ cross section. For $p\bar{p}\to W\to e\nu\gamma$, on the other hand, it is the most severe cut. We will discuss in Sec. IV B the extent to which the $\Delta R_{e\gamma}>0.7$ requirement limits the measurements of $WW\gamma$ couplings in radiative W decays.

The cuts we impose simulate detector response only roughly. Within the cuts listed in (3.7) and with an integrated luminosity of 100 pb^{-1} the Tevatron will provide about 140 $W^{\pm}\to e^{\pm}\nu\gamma$ events with a well-separated $e^{\pm}\gamma$ pair, and about 50 clean $W^{\pm}\gamma$, $W^{\pm}\to e^{\pm}\nu$ events in a $p_{T\gamma}$ and η_γ range which is particularly sensitive to anomalies in the $WW\gamma$ vertex.

IV. SIGNATURES FOR ANOMALOUS $WW\gamma$ COUPLINGS

A. $W\gamma$ production

In the $q\bar{q}'\to W\gamma$ subprocess the effects of anomalies in the $WW\gamma$ vertex are enhanced at large energies, due to

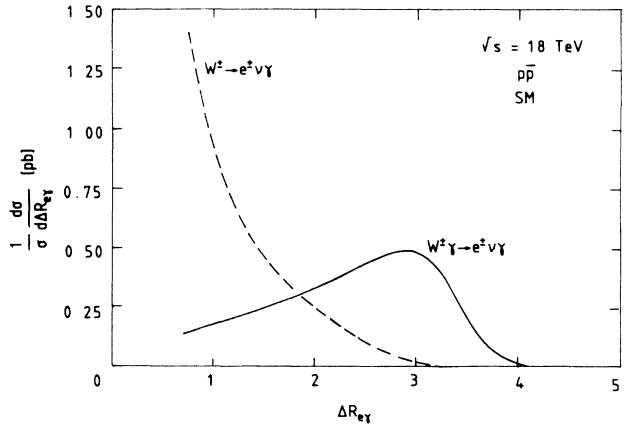

FIG. 3. Normalized distribution $(1/\sigma)(d\sigma/d\Delta R_{e\gamma})$ of the electron-photon separation $\Delta R_{e\gamma}$ in $p\bar{p}\to W^{\pm}\gamma$, $W^{\pm}\to e^{\pm}\nu$ [solid line; $M_T(e\gamma;\not{p}_T)>90$ GeV] and $p\bar{p}\to W^{\pm}\to e^{\pm}\nu\gamma$ [dashed line; $M_T(e\gamma;\not{p}_T)<90$ GeV] at $\sqrt{s}=1.8$ TeV in the SM. The cuts specified in Eq. (3.7) are imposed. QCD corrections are simulated by a K factor.

the $\hat{\gamma}=\sqrt{\hat{s}}/2M_W$ factors in the anomalous contributions to the amplitudes (2.4). This enhancement factor will particularly favor the observability of anomalous values of λ and $\tilde{\lambda}$, which are enhanced by $\hat{\gamma}^2$ in the amplitude whereas terms containing κ and $\tilde{\kappa}$ grow only linearly with $\hat{\gamma}$.

A typical signal for anomalous couplings will be a broad increase in the W-photon invariant-mass spectrum at large values of $M_{W\gamma}=\sqrt{\hat{s}}$. The resulting effect on $Bd\sigma/dM_{W\gamma}$ is shown in Fig. 4 for the illustrative values $\Delta\kappa=\kappa-1=1$ and $\lambda=0.5$. Only one $WW\gamma$ coupling at a time is chosen different from the SM prediction. For comparison the SM curve is included as a solid line.

At hadron colliders the $W\gamma$ invariant mass cannot be determined unambigously because the neutrino from W decay is not observed. If the transverse momentum of the neutrino is identified with the missing transverse momentum of a given $W\gamma$ event, the unobservable longitudinal neutrino momentum $p_{L\nu}$ can be reconstructed, albeit with a twofold ambiguity, by imposing the constraint that the neutrino and the electron four-momenta combine to form the W rest mass.[8,34] Neglecting the electron mass one finds

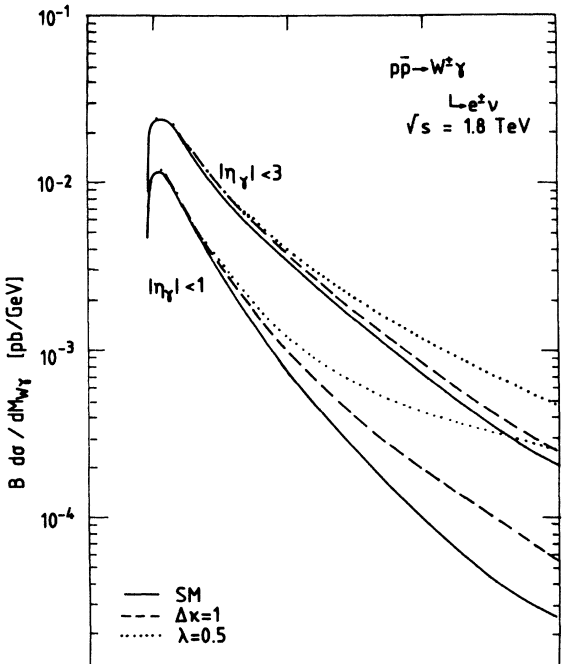

FIG. 4. W photon invariant-mass spectrum for the process $p\bar{p}\to W^{\pm}\gamma$, $W^{\pm}\to e^{\pm}\nu$ at the Tevatron. The curves are for the SM (solid curves), $\Delta\kappa=\kappa-1=1$ (dashed curves), and $\lambda=0.5$ (dotted curves). The lower solid, dashed, and dotted curve give the results for the cuts of Eq. (3.7). The upper solid, dashed, and dotted curves show the $M_{W\gamma}$ spectrum with the $|\eta_\gamma|<1$ cut of (3.7) replaced by $|\eta_\gamma|<3$, and all other cuts unchanged. Higher-order QCD corrections are approximated by a K factor.

$$p_{L\nu}=\frac{1}{2p_{Te}^2}\{p_{Le}(M_W^2+2\mathbf{p}_{Te}\cdot\not{\mathbf{p}}_T)\pm p_e[(M_W^2+2\mathbf{p}_{Te}\cdot\not{\mathbf{p}}_T)^2-4\not{p}_T^2p_{Te}^2]^{1/2}\}\ , \quad (4.1)$$

where p_{Le} denotes the electron longitudinal momentum. Plotted in Fig. 4 is the "reconstructed" $W\gamma$ invariant-mass spectrum obtained from the two solutions for $p_{L\nu}$ for each event.

In Fig. 4 the anomalous coupling curves are clearly distinguishable from the SM prediction. For the expected integrated luminosity of 100 pb^{-1} for future Tevatron runs, a differential cross section of 10^{-4} pb/GeV corresponds to one event per 100 GeV interval. Since terms in the helicity amplitudes which are proportional to λ grow much faster ($\sim\hat{\gamma}^2$) than κ terms ($\sim\hat{\gamma}$) for $\sqrt{\hat{s}}\gg M_W$, the $M_{W\gamma}$ spectrum for anomalous values of λ is much harder than the one for a nonstandard κ.

In addition to the curves for the standard set of cuts [Eq. (3.7)], Fig. 4 also shows the $M_{W\gamma}$ distribution with the $|\eta_\gamma|<1$ cut replaced by $|\eta_\gamma|<3$. The increase of the cross section at large $M_{W\gamma}$ due to anomalous $WW\gamma$ couplings is much more pronounced for $|\eta_\gamma|<1$ than for $|\eta_\gamma|<3$. This is the reason we have chosen the rather stringent cut of $|\eta_\gamma|<1$ in (3.7). For $|\eta_\gamma|>1$ $W\gamma$ production at the Tevatron is insensitive to anomalous $WW\gamma$ couplings. As far as a measurement of the $WW\gamma$ vertex is concerned, the only use of the $|\eta_\gamma|>1$ data is to provide a check on the normalization of the $W\gamma$ production cross section.

At the Tevatron the sensitivity to anomalous couplings in $p\bar{p}\to W\gamma$ effectively stems from regions in phase space where the anomalous contributions to the cross section are considerably larger than the SM expectation. As a result, interference effects between the SM amplitude and the anomalous amplitude contributions (2.4) play a minor role, and an excess in counting rate, beyond the SM prediction, scales essentially like the square of the anomalous coupling.

As we shall see in Sec. V, existing low-energy bounds limit $|\tilde{\kappa}|$ to less than $\sim 10^{-3}$, and no visible effects of $\tilde{\kappa}$ are possible at the Tevatron. Because contributions to the helicity amplitudes containing λ and $\tilde{\lambda}$ differ only by a factor $\pm i$, cross sections for the same values of λ and $\tilde{\lambda}$ are almost identical. Results for anomalous $\tilde{\kappa}$ and $\tilde{\lambda}$ values are therefore not included in Fig. 4 and all subsequent figures.

As already mentioned, the $W\gamma$ differential cross section vanishes, in the SM, at one value of the photon scattering angle. For $u\bar{d}\to W^+\gamma$ ($d\bar{u}\to W^-\gamma$) the radiation zero occurs at $\cos\theta^*=-\frac{1}{3}$ ($+\frac{1}{3}$), where θ^* is the scattering angle of the photon relative to the quark direction, in the $W\gamma$ center-of-mass frame. In practice, however, the zero is washed out considerably. In order to measure θ^* the $W\gamma$ rest frame has to be reconstructed. Since the unobservable longitudinal neutrino momentum can only be determined with a twofold ambiguity and, on an event to event basis, one does not known which solution is the correct one, both solutions have to be considered for each event and the zero is partially filled in. A similar effect is caused by the small fraction of radia-

tive W decay events which passes the $W\gamma$ selection cuts[6] and by the fact that one does not know whether one has to associate the quark with the proton or the antiproton. Finally, when one sums over the W charges, only $|\cos\theta^*|$ remains measurable, and the dip at $\cos\theta^* = \pm\frac{1}{3}$ is shifted to $\cos\theta^* = 0$.

In order to eliminate the strong peaking of the differential cross section at $\cos\theta^* = \pm 1$ which arises from the collinear singularity, it is convenient instead to study the rapidity distribution $B\, d\sigma/d|y^*|$ of the photon in the $W\gamma$ rest frame,[11] with

$$y^* = \tfrac{1}{2}\ln\frac{1+\cos\theta^*}{1-\cos\theta^*} . \tag{4.2}$$

The resulting distribution is shown in Fig. 5 for the same anomalous couplings as in Fig. 4. For each event both values of y^* are plotted corresponding to the twofold ambiguity in the neutrino longitudinal momentum. The dip at $|y^*| = 0$, which is due to the radiation zero, is quite pronounced. In presence of any anomalous contribution to the $WW\gamma$ vertex the radiation zero is eliminated and the dip is filled at least partially.

Compared with the effects discussed above which obscure the radiation zero, the effect induced by higher-order QCD corrections is small.[12] Soft QCD corrections which can be approximated by a K factor exhibit the same radiation zero as the Born cross section. These effects are taken into account in our calculation. Hard QCD corrections which result in a finite p_T for the $W\gamma$ system are found to influence the radiation zero insignificantly at Tevatron energies.[12]

As discussed in Sec. III, the W jet background does not pose problems at the Tevatron for $p_{T\gamma} < 50$ GeV whereas for transverse momenta bigger than 50 GeV it cannot be neglected *a priori*. The dashed-dotted line in Fig. 5 shows the y^* distribution for $p\bar{p} \to W^{\pm}$ jet, calculated with $p_{Tj} > 50$ GeV and the cuts specified in Eq. (3.7). To represent the misidentification probability $P_{\gamma/j}$ of a jet as a photon the W jet y^* spectrum was multiplied by a factor 5×10^{-3}. In view of our discussion in Sec. III this value can be considered a safe upper limit for $P_{\gamma/j}$. Hence, our estimate of the W jet background is conservative. From Fig. 5 we observe that the background is considerably smaller than the SM $W\gamma$ cross section over the entire y^* range. Although the W jet cross section peaks at $y^* = 0$, and thus tends to fill in the dip caused by the radiation zero, we conclude that the W jet background for $p_{Tj} > 50$ GeV does not severely limit the sensitivity of the y^* distribution to anomalous couplings. A similar result is also obtained for other distributions which are sensitive to anomalous contributions to the $WW\gamma$ vertex.

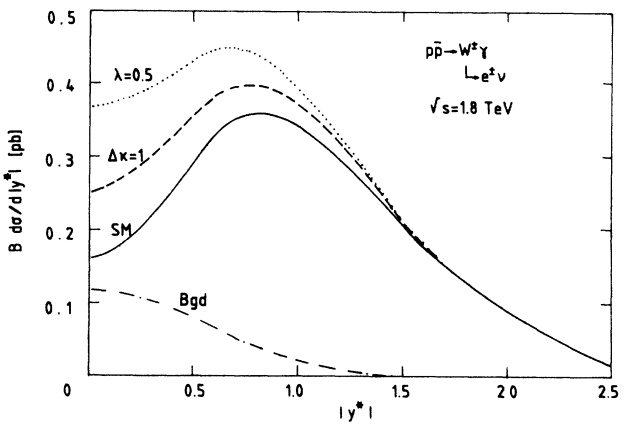

FIG. 5. Rapidity spectrum of the photon in the $W\gamma$ rest frame for $p\bar{p} \to W^{\pm}\gamma$, $W^{\pm} \to e^{\pm}\nu$ at the Tevatron. The anomalous couplings are the same as in Fig. 4. Cuts are specified in Eq. (3.7). The dashed-dotted line represents the background from $W^{\pm}$ jet production (see text for details). QCD corrections

Figure 5 demonstrates that anomalous couplings affect mainly the region of small center-of-mass rapidities. This is due to the fact that anomalous couplings only contribute via the s-channel W-exchange graph of Fig. 1, and hence only to the $J = 1$ partial wave, when fermion masses are neglected. The anomalous contributions are, therefore, almost isotropic in the center-of-mass frame, while the u- and t-channel graphs of Fig. 1 result in a strong enhancement of the high-rapidity region. Thus the finite acceptance cuts will largely eliminate the well-known fermion-exchange contributions to the cross section and reduce by a much smaller amount possible signals of new physics, i.e., the effects of anomalous $WW\gamma$ interactions. This is evident also from Fig. 4.

The population of the small rapidity region, induced by anomalous couplings, considerably increases the average photon transverse momentum of events produced at a fixed value of the W photon invariant mass. The p_T distribution of the photon, $d\sigma/dp_{T\gamma}$, should be particularly sensitive to anomalous couplings. This fact is visible in Fig. 6 where the $p_{T\gamma}$ spectrum is plotted for the SM, and for $\Delta\kappa = 1$ and $\lambda = 0.5$. For an integrated luminosity of 100 pb^{-1}, experiments at the Tevatron should be able to see the effect.

As we have demonstrated so far, the $W\gamma$ invariant-mass spectrum, the rapidity distribution of the produced photon in the $W\gamma$ rest frame, and the photon transverse-momentum spectrum are sensitive indicators of anomalous couplings. We now want to make these statements more quantitative by deriving those values of κ, λ, and $\tilde{\lambda}$ which would give rise to a deviation from the SM at the 90% (69%) confidence level (C.L.) in either the $M_{W\gamma}$, the y^* or the $p_{T\gamma}$ spectrum. We assume an integrated luminosity of $\int \mathcal{L}\, dt = 100$ pb^{-1} at the Tevatron and the cuts of Eq. (3.7). The parameter $\tilde{\kappa}$ is omitted since, as already mentioned, low-energy data constrain this quantity to be less than $\sim 10^{-3}$. The confidence level is calculated by splitting the $M_{W\gamma}$ and y^* distributions into six bins each and the $p_{T\gamma}$ distribution into five bins with, typically, more than five events. In each bin the Poisson statistics is approximated by a Gaussian distribution. In order to achieve a sizable counting rate in each bin, all events with $M_{W\gamma} > 140$ GeV and $p_{T\gamma} > 30$ GeV are collected into a single bin. This procedure guarantees that in our calculation a high confidence level cannot arise from a single event at high $M_{W\gamma}$ or $p_{T\gamma}$ where the SM predicts, say,

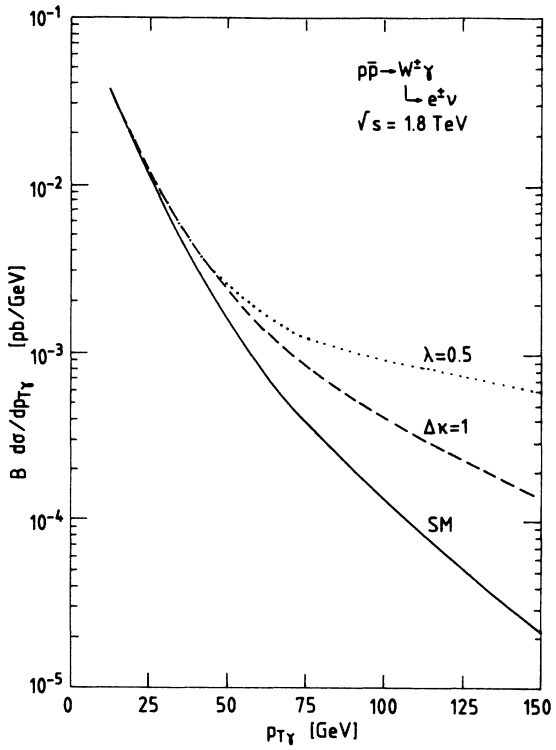

FIG. 6. Transverse-momentum spectrum of the photon in $p\bar{p}\to W^{\pm}\gamma$, $W^{\pm}\to e^{\pm}\nu$ at the Tevatron. Parameters and cuts are chosen as in Fig. 5. A K factor is used to simulate QCD corrections.

only 0.01 events. In order to derive realistic limits we include the W jet background for $p_{Tj}>50$ GeV in our analysis and allow for a normalization uncertainty $\Delta\mathcal{N}$ of the SM $W\gamma$ production cross section of $\Delta\mathcal{N}=50\%$. QCD corrections are simulated by a K factor.

The resulting minimal anomalous couplings which would give rise to a 90% or 69% C.L. effect at the Tevatron are given in Table I. Only one coupling at a time is assumed to be different from the SM value. The sensitivity bounds are given for two choices of the photon-jet misidentification probability, $P_{\gamma/j}=5\times10^{-3}$ and a somewhat more optimistic value of $P_{\gamma/j}=5\times10^{-4}$. These two values were chosen in order to display the effect of the W jet background on the limits that can be achieved.

In all cases the p_T spectrum of the photon is the most sensitive indicator of anomalous couplings. This can be easily understood by remembering that $d\sigma/dM_{W\gamma}$ as well as $d\sigma/d|y^*|$ both depend on the reconstructed longitudinal momentum $p_{L\nu}$ of the neutrino whereas this is not the case of the $p_{T\gamma}$ spectrum. Since $p_{L\nu}$ can only be determined with a twofold ambiguity [see Eq. (4.1)], the effects of anomalous $WW\gamma$ couplings are less pronounced in the $M_{W\gamma}$ and y^* distributions than in the $p_{T\gamma}$ spectrum.

Table I shows that λ and $\tilde{\lambda}$ can be measured with 25–40% accuracy with an integrated luminosity of 100 pb^{-1} if $P_{\gamma/j}=5\times10^{-4}$. These errors become larger by roughly 20% if $P_{\gamma/j}=5\times10^{-3}$. On the other hand, $|\Delta\kappa|$ can only be constrained to be less than 0.8–1.5. The values presented in Table I thus directly reflect the different powers of $\hat{\gamma}=\sqrt{\hat{s}}/2M_W$ multiplying the various anomalous contributions to the amplitudes (2.4). At high energies ($\hat{s}\gg M_W^2$) terms proportional to λ and $\tilde{\lambda}$ grow much faster than κ terms, and the sensitivity limits achievable for λ and $\tilde{\lambda}$ are thus considerably better than the ones for κ. Since interference effects between the SM amplitude and the anomalous contributions (2.4) to the amplitudes play only a minor role, the limits in Table I do not depend significantly on the sign of the anomalous coupling. Furthermore, the limits for λ and $\tilde{\lambda}$ are very similar because terms in the helicity amplitudes containing λ and $\tilde{\lambda}$ differ only by a factor $\pm i$.

The bounds presented in Table I have been derived by assuming that only one coupling at a time deviates from the SM. Since the leading contributions to the helicity amplitudes which are proportional to κ and λ grow with different powers of $\sqrt{\hat{s}}/M_W$ [see Eq. (2.4)], effects of anomalous values of κ and λ cannot cancel at a significant level in the $p\bar{p}\to W\gamma$ distributions. Taking into account possible cancellations between terms proportional to $\Delta\kappa$ and λ in the helicity amplitudes, we find that the bounds given in Table I increase by at most 30%. Terms in (2.4) containing the CP-violating coupling $\tilde{\lambda}$ contribute imaginary parts to the helicity amplitudes. Because the CP-conserving parts are real, all interference effects between $\tilde{\lambda}$ and $\kappa(\lambda)$ terms vanish identically. Hence the sensitivities of Table I represent model-independent upper bounds that can be set by experiments.

TABLE I. Sensitivities achievable at the 90% and 69% C.L. for the anomalous $WW\gamma$ couplings $\Delta\kappa=\kappa-1$, λ, and $\tilde{\lambda}$ in $p\bar{p}\to W^{\pm}\gamma$, $W^{\pm}\to e^{\pm}\nu$ at the Tevatron ($\sqrt{s}=1.8$ TeV) for an integrated luminosity of 100 pb^{-1}. The bounds are given for a photon-jet misidentification probability of $P_{\gamma/j}=5\times10^{-3}$ and $P_{\gamma/j}=5\times10^{-4}$. Only one coupling at a time is assumed to be different from the SM value.

	$\Delta\kappa$		λ		$\tilde{\lambda}$	
$P_{\gamma/j}$	5×10^{-3}	5×10^{-4}	5×10^{-3}	5×10^{-4}	5×10^{-3}	5×10^{-4}
90% C.L.	+1.50	+1.23	+0.46	+0.38	+0.46	+0.39
	−1.41	−1.13	−0.47	−0.40	−0.46	−0.39
69% C.L.	+0.99	+0.82	+0.30	+0.25	+0.31	+0.26
	−0.90	−0.72	−0.31	−0.26	−0.31	−0.26

Table I has been derived from $p\bar{p} \to W^{\pm}\gamma$; $W^{\pm} \to e^{\pm}\nu$. Including the decay $W^{\pm} \to \mu^{\pm}\nu$ would increase statistics by less than a factor 2, due to the smaller efficiency in detecting muons. Hence, the statistical error would be reduced by less than a factor $\sqrt{2}$ and the sensitivity to any of the anomalous couplings would improve by less than a factor $2^{1/4}$, i.e., 20%.

B. Radiative W decays

The sensitivity of radiative W decays to anomalous contributions to the $WW\gamma$ vertex results mostly from the radiation zero which, in the SM, is present in the angular distribution of the photon in the W center-of-mass frame. For $W \to e\nu\gamma$ the radiation zero occurs at $\cos\theta^*_{e\gamma} = -1$, where $\theta^*_{e\gamma}$ is the angle between the electron and the photon in the W rest frame.

In practice, the zero is washed out considerably. In order to measure $\theta^*_{e\gamma}$ the W center-of-mass frame has to be determined. This cannot be done unambigously since the neutrino in $W \to e\nu\gamma$ is not observed. If the transverse momentum of the neutrino is identified with the $\not{p}_T$ of a given $W \to e\nu\gamma$ event, the unobservable longitudinal momentum of the neutrino can be reconstructed by requiring that the neutrino, the electron, and the photon four-momenta combine to form the W rest mass.[8] Similar to the reconstruction of $p_{L\nu}$ in $W\gamma$ production this procedure results in a twofold ambiguity. One finds

$$p_{L\nu} = \frac{1}{2(E^2_{e\gamma} - P^2_{Le\gamma})} \{ p_{Le\gamma}(M^2_W - M^2_{e\gamma} + 2\mathbf{p}_{Te\gamma} \cdot \not{\mathbf{p}}_T) \pm E_{e\gamma}[(M^2_W - M^2_{e\gamma} + 2\mathbf{p}_{Te\gamma} \cdot \not{\mathbf{p}}_T)^2 - 4\not{p}^2_T (E^2_{e\gamma} - p^2_{Le\gamma})]^{1/2} \} , \tag{4.3}$$

where

$$\begin{aligned} E_{e\gamma} &= E_e + E_\gamma , \\ p_{Le\gamma} &= p_{Le} + P_{L\gamma} , \\ \mathbf{p}_{Te\gamma} &= \mathbf{p}_{Te} + \mathbf{p}_{T\gamma} \end{aligned} \tag{4.4}$$

are the energy, the longitudinal, and the transverse momenta of the $e\gamma$ system, and $M_{e\gamma}$ denotes the $e\gamma$ invariant mass.

Because of the ambiguity in $p_{L\nu}$ the radiation zero is partially filled in. A similar effect is also caused by finite-W-width effects and by the small fraction of $W\gamma$ events which passes the selection cuts for $p\bar{p} \to W^{\pm} \to e^{\pm}\nu\gamma$ (Ref. 6). The resulting $\cos\theta^*_{e\gamma}$ spectrum is shown in Fig. 7 for the SM case (solid line) and the illustrative values $\Delta\kappa = 3$ (dashed line) and $\lambda = 2$ (dotted line). The dominant contribution to $p\bar{p} \to W \to e\nu\gamma$ arises from the graphs in Figs. 1(d) and 1(e) which leads to a singularity at $\cos\theta^*_{e\gamma} = +1$. Thus a strong peaking of the cross section results in the forward direction. Since the $WW\gamma$ vertex does not enter this diagram, the $p\bar{p} \to W \to e\nu\gamma$ cross section for small $\theta^*_{e\gamma}$ is insensitive to anomalous $WW\gamma$ couplings, and no sensitivity is lost by requiring the electron and the photon to be well isolated. The

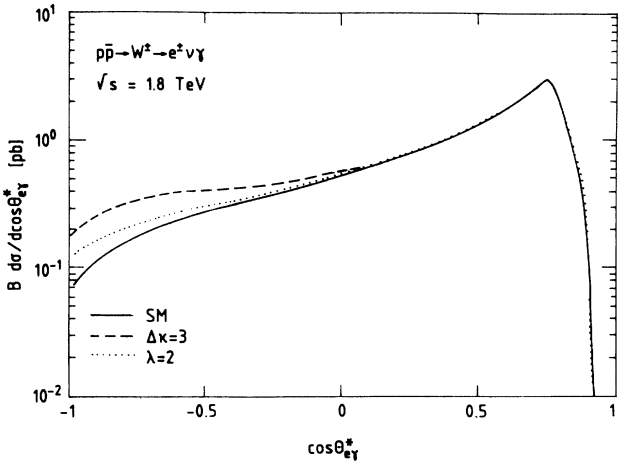

FIG. 7. Distribution of the angle between the electron and the photon in the W rest frame, $\theta^*_{e\gamma}$, for $p\bar{p} \to W^{\pm} \to e^{\pm}\nu\gamma$ at the Tevatron, with the cuts specified in Eq. (3.7). The curves are for the SM (solid line), $\Delta\kappa = 3$ (dashed line), and $\lambda = 2$ (dotted line). Higher-order QCD corrections are approximated by a K factor.

effect of the $\Delta R_{e\gamma} > 0.7$ cut is clearly visible in Fig. 7: for $\cos\theta^*_{e\gamma} > 0.8$ the cross section falls off very rapidly and vanishes for values bigger than 0.92. In the region of the radiation dip, on the other hand, the $\cos\theta^*_{e\gamma}$ distribution is sensitive to deviations from the SM. If anomalous couplings are present, the dip is filled in at least partially.

The cuts applied in Fig. 7 are summarized in Eq. (3.7). If the photon pseudorapidity cut is relaxed to $|\eta_\gamma| < 3$ the enhancement of the cross section at $\cos\theta^*_{e\gamma} = -1$ for non-gauge-theory $WW\gamma$ couplings would be less pronounced than for $|\eta_\gamma| < 1$.

QCD corrections are not expected to influence the shape of the $\cos\theta^*_{e\gamma}$ distribution significantly. Effects induced by the transverse motion of the W can be easily corrected for since the p_T spectrum of the W is known from $W \to e\nu, \mu\nu$ decays.[6] Furthermore, $\theta^*_{e\gamma}$ is defined in the W rest frame and, therefore, does not depend on the p_T of the W in first approximation.

The counting rate for $\cos\theta^*_{e\gamma} \approx -1$ is strongly influenced by the $\not{p}_T$ cut imposed. In Fig. 8, the SM $p\bar{p} \to W^{\pm} \to e^{\pm}\nu\gamma$ cross section is plotted versus $\cos\theta^*_{e\gamma}$ for three different values of minimal $\not{p}_T$. One observes that the rate for $\not{p}_T > 10$ GeV is almost a factor 3 larger than for $\not{p}_T > 20$ GeV. The same qualitative behavior is found for anomalous couplings. The variation of the counting rate with the $\not{p}_T$ cut at $\cos\theta^*_{e\gamma} = -1$ can be understood from the kinematics of the $e\nu\gamma$ system. If the electron and the photon are back to back, either the neutrino and the photon, or the neutrino and the electron are collinear, i.e.,

$$p_{Te} = \not{p}_T + p_{T\gamma} \quad \text{for } \cos\theta^*_{e\gamma} = -1 , \tag{4.5a}$$

or

$$p_{T\gamma} = \not{p}_T + p_{Te} \quad \text{for } \cos\theta^*_{e\gamma} = -1 . \tag{4.5b}$$

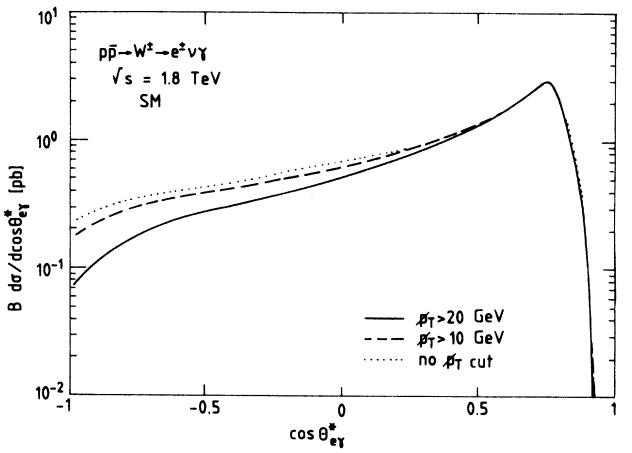

FIG. 8. Distribution of the angle between the electron and the photon in the W rest frame, $\theta^*_{e\gamma}$, for $p\bar{p}\to W^{\pm}\to e^{\pm}\nu\gamma$ at the Tevatron in the SM. The curves are for $\not{p}_T > 20$ GeV (solid line), $\not{p}_T > 10$ GeV (dashed line), and no $\not{p}_T$ cut (dotted line). All other cuts are as specified in Eq. (3.7). QCD corrections are simulated by a K factor.

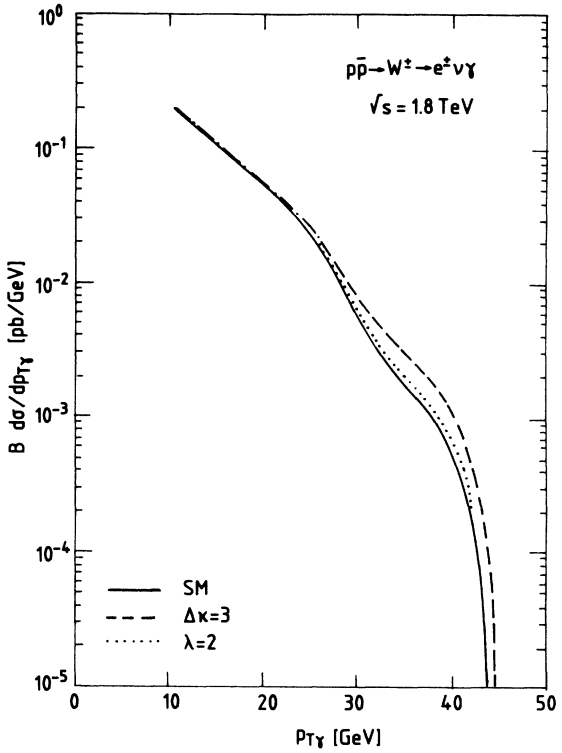

FIG. 9. Transverse-momentum spectrum of the photon in $p\bar{p}\to W^{\pm}\to e^{\pm}\nu\gamma$ at the Tevatron. Parameters and cuts are chosen as in Fig. 7. A K factor is used to simulate QCD corrections.

For the cuts specified in Eq. (3.7), at $\cos\theta^*_{e\gamma} = -1$, either $p_{Te} > 30$ GeV or $p_{T\gamma} > 35$ GeV. Both requirements suppress the rate substantially.

The population of the dip region in the $\cos\theta^*_{e\gamma}$ distribution, induced by the anomalous couplings, will lead to an excess of events at large values of $p_{T\gamma}$ and p_{Te}. The excess is shown in Fig. 9 where the transverse-momentum spectrum of the photon is plotted for the SM, $\Delta\kappa = 3$ and $\lambda = 2$. Qualitatively and quantitatively similar effects are obtained for $d\sigma/dp_{Te}$.

If the electron and the photon are back to back, the invariant mass $M_{e\gamma}$ of the $e\gamma$ system tends to be large. We therefore expect that anomalies in the $WW\gamma$ vertex result in a broad increase in the $e\gamma$ invariant-mass spectrum at large values of $M_{e\gamma}$. This effect is displayed in Fig. 10 for the same anomalous couplings as in Fig. 7.

The results in Figs. 7, 9, and 10 show that radiative W decays are much less sensitive to anomalous couplings than W-photon production. Thus, rather large anomalies in the $WW\gamma$ vertex are necessary in order to produce a measurable effect in $p\bar{p}\to W^{\pm}\to e^{\pm}\nu\gamma$. In Table II we list those values of $\Delta\kappa$, λ, and $\tilde{\lambda}$ which result in a deviation from the SM at the 90% (69%) confidence level for $\int\mathcal{L}\,dt = 100$ pb^{-1} at the Tevatron in the $p_{T\gamma}$, the $\cos\theta^*_{e\gamma}$ or the $M_{e\gamma}$ spectrum. The procedure used to calculate the confidence levels is analogous to the one used in deriving the bounds of Table I. The $p_{T\gamma}$, $\cos\theta^*_{e\gamma}$, and $M_{e\gamma}$ spectrum are split into 8, 6, and 7 bins, respectively. To achieve a sufficient number of events in each bin, all events with $p_{T\gamma} > 24$ GeV, $\cos\theta^*_{e\gamma} > 0.8$, and $M_{e\gamma} > 44$ GeV are combined in a single bin. Furthermore, we allow for a normalization uncertainty of the SM $p\bar{p}\to W\to e\nu\gamma$ rate of $\Delta\mathcal{N} = 50\%$ and include a K factor to account for higher-order QCD effects. Since $p_{T\gamma} < \frac{1}{2}M_W \approx 40$ GeV in radiative W decays, the W jet

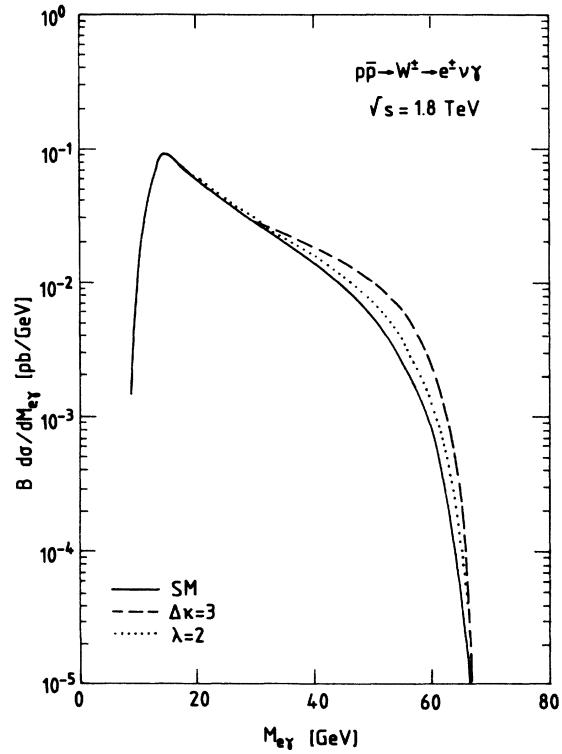

FIG. 10. Electron-photon invariant-mass spectrum for $p\bar{p}\to W^{\pm}\to e^{\pm}\nu\gamma$ at the Tevatron. Parameters and cuts are chosen as in Fig. 7. QCD corrections are simulated by a K factor.

TABLE II. Sensitivities achievable at the 90% and 69% C.L. for the anomalous $WW\gamma$ couplings $\Delta\kappa=\kappa-1$, λ, and $\tilde{\lambda}$ in $p\bar{p}\to W^{\pm}\to e^{\pm}\nu\gamma$ at the Tevatron ($\sqrt{s}=1.8$ TeV) for an integrated luminosity of 100 pb^{-1}. Only one coupling at a time is assumed to be different from the SM value.

	$\Delta\kappa$	λ	$\tilde{\lambda}$
90% C.L.	+2.42	+3.19	+3.37
	−2.48	−3.00	−3.37
69% C.L.	+1.67	+2.23	+2.33
	−1.72	−2.06	−2.33

background is expected to pose no problem (see Sec. III) and, therefore, is not included in our calculation of sensitivity limits resulting from $p\bar{p}\to W\to e\nu\gamma$.

The $M_{e\gamma}$ spectrum provides the highest confidence levels for all three anomalous couplings considered. Since the SM helicity amplitudes vanish at the radiation zero, interference effects between the anomalous contributions to the helicity amplitudes and the SM part again play a minor role only, and the limits do not depend significantly on the sign of the anomalous coupling. The bounds presented in Table II are considerably weaker than the limits expected from $W\gamma$ production (see Table I), in particular for λ and $\tilde{\lambda}$. Most of the sensitivity of W-photon production to anomalous $WW\gamma$ couplings results from the high-energy region ($\hat{s}\gg M_W^2$) where the anomalous contributions to the helicity amplitudes dominate the SM part. This region is not accessible in radiative W decays where $\sqrt{\hat{s}}\approx M_W$, and the sensitivity to anomalous couplings in $p\bar{p}\to W\to e\nu\gamma$ originates mostly from the radiation zero at $\cos\theta^*_{e\gamma}=-1$. However, finite-$W$-width effects and the ambiguity in reconstructing the longitudinal momentum of the neutrino obscure the radiation zero considerably, resulting in rather poor limits on $\Delta\kappa$, λ, and $\tilde{\lambda}$.

The bounds presented in Table II could be improved somewhat if the $\not{p}_T>20$ GeV cut could be lowered to $\not{p}_T>10$ GeV. This would increase the counting rate at $\cos\theta^*_{e\gamma}=-1$ by about a factor 3 (see Fig. 8) and thus improve the limits by roughly 30%. Nevertheless, the bounds on the anomalous $WW\gamma$ couplings from $W\to e\nu\gamma$ would still be significantly weaker than those from $W\gamma$ production.

In deriving the limits listed in Table II we have assumed that only one coupling at a time differs from the SM value. Because the center-of-mass energy in radiative W decays is fixed ($\sqrt{\hat{s}}\approx M_W$), larger cancellations between terms proportional to $\Delta\kappa$ and λ in the helicity amplitudes may occur if both couplings deviate from their SM values at the same time. Cancellation could result in limits for $\Delta\kappa$ and λ which are considerably weaker than the ones given in Table II. Since the bounds on anomalous $WW\gamma$ couplings from $W\gamma$ production are much stronger than the limits which can be derived from radiative W decays, we have not analyzed in detail the effects induced by the cancellation of κ and λ terms.

V. DISCUSSION AND CONCLUSIONS

We have described the signatures which anomalies in the $WW\gamma$ vertex will produce in $W\gamma$ production and radiative W decays at the Tevatron. In particular we have determined how large deviations from the SM must be in order to yield visible effects for an integrated luminosity of $\int\mathcal{L}\,dt=100$ pb.$^{-1}$. It is interesting to compare the sensitivity of the Tevatron with existing low-energy limits on anomalous couplings and with the sensitivity to non-gauge-theory terms in the $WW\gamma$ vertex accessible via $e^+e^-\to W^+W^-$ at CERN LEP 200, and via single W production in ep collisions at DESY HERA.

Low-energy bounds on κ and λ are quite model dependent at present.[19] From loop contributions to $(g-2)_\mu$ (Ref. 20) one estimates

$$\left|(\kappa-1)\ln\frac{\Lambda^2}{M_W^2}+\frac{\lambda}{3}\right|<3.7\ , \tag{5.1}$$

where Λ is the scale at which weak bosons show novel strong interactions. Bounds derived from the photon propagator as measured at DESY PETRA (Ref. 15) and the W/Z mass ratio[14,15] are more stringent, but also more controversial because loop corrections are ill defined in these cases. From Table I we may conclude that experiments at the Tevatron can significantly improve the present low-energy bound on λ, derived from $(g-2)_\mu$. For κ the low-energy level of accuracy can be reached. The situation is quite different for the CP-violating coupling $\tilde{\kappa}$ which would contribute to the electric dipole moment of the neutron. From the present experimental limit on the neutron electric dipole moment one finds[17]

$$\left|\tilde{\kappa}\ln\frac{\Lambda^2}{M_W^2}\right|<10^{-3} \tag{5.2}$$

which clearly excludes any observable effect at the Tevatron. Curiously, as was observed in Ref. 18, no such bound exists for the other CP-violating coupling $\tilde{\lambda}$. Contributions of $\tilde{\lambda}$ to the neutron electric dipole moment are suppressed by at least another factor $(M_N^2/M_W^2)\approx 1.3\times10^{-4}$ (M_N being the neutron mass) compared to the $\tilde{\kappa}$ bound (5.2) and hence a constraint $|\tilde{\lambda}|\lesssim 1$ results at best. Comparison with Table I shows that the Tevatron would be able to explore almost one order of magnitude in $\tilde{\lambda}$. Of course, hadron supercolliders such as the CERN Large Hadron Collider (LHC) or the Superconducting Super Collider (SSC) would be even more sensitive to λ and $\tilde{\lambda}$. At these machines λ ($\tilde{\lambda}$) values as small as $\sim10^{-3}$ can be probed.[11]

Our analysis shows that a detailed investigation of radiative W decays and W-photon production at Tevatron energies requires an integrated luminosity of at least 100 pb^{-1}. Nevertheless, a few events of each type may already be found in the present data set. For $\int\mathcal{L}\,dt=4.7$ pb^{-1} one expects 7 $W^{\pm}\to e^{\pm}\nu\gamma$ and 2 $W^{\pm}\gamma$; $W^{\pm}\to e^{\pm}\nu$ events within the cuts of Eq. (3.7). If the pseudorapidity cut of the photon is relaxed to $|\eta_\gamma|<3$, the events rates grow by about a factor 1.5 and 3, respectively. Since the expected number of $W\gamma$ events is very small, the only

meaningful observable which can be used to derive bounds on the anomalous couplings from present Tevatron data is the total $W\gamma$ cross section within cuts. Assuming that only one coupling at a time differs from the gauge theory value and that the SM $p\bar{p}\to W\gamma$ rate can be determined within 50%, sensitivities of

$$\begin{aligned}\Delta\kappa &= \begin{cases}+3.1\ (+5.6),\\ -2.9\ (-5.4).\end{cases}\\ \lambda &= \pm 1.1\ (\pm 2.1)\ ,\\ \tilde{\lambda} &= \pm 1.1\ (\pm 2.1)\end{aligned} \tag{5.3}$$

can be reached at the 1σ (5σ) level from the total $p\bar{p}\to W\gamma$; $W\to e\nu$ cross section with an integrated luminosity of 4.7 pb^{-1}. For $\Delta\kappa$ these limits are weaker than the bound implied by Eq. (5.1). For λ, on the other hand, a significantly stronger limit than from $(g-2)_\mu$ results. The $\tilde{\lambda}$ limit which can be reached with present Tevatron data appears to be competitive with the bound which can be obtained from the electric dipole moment of the neutron.

The UA2 Collaboration at the CERN $p\bar{p}$ collider should also find a few $e^{\pm}\gamma\not{p}_T$ events in the data recorded during the last run. At $\sqrt{s}=630$ GeV the cross section for $p\bar{p}\to W^{\pm}\to e^{\pm}\nu\gamma$ ($p\bar{p}\to W^{\pm}\gamma$, $W^{\pm}\to e^{\pm}\nu$) is 2.0 pb (0.3 pb) for cuts which roughly simulate the response of the UA2 detector[35] ($p_{T\gamma}>10$ GeV, $p_{Te}>15$ GeV, $|\eta_{\gamma,e}|<2$, $\not{p}_T>15$ GeV and $\Delta R_{e\gamma}>0.3$). For an integrated luminosity of 7 pb^{-1} one thus expects about 14 radiative W decay and 2 W-photon events in the UA2 sample. The limits on non-gauge-theory terms in the $WW\gamma$ vertex which can be obtained from present UA2 data are significantly weaker than the ones from the Tevatron, due to the much smaller range of center of mass energies at the CERN $p\bar{p}$ collider.

Experiments at HERA, studying single W production via $ep\to eWX$, will also be able to probe the $WW\gamma$ vertex.[36] In ep collisions at $\sqrt{s}=314$ GeV, for an integrated luminosity of 10^3 pb^{-1}, one expects about 90 $ep\to eW^{\pm}X$ events with $W\to e\nu,\mu\nu$. It turns out that HERA is considerably more sensitive to κ than to λ and $\tilde{\lambda}$. While κ can be measured with 30–50 % accuracy, $|\lambda|$ and $|\tilde{\lambda}|$ can only be constrained to be less than 0.9–1.3 (Ref. 36). HERA will thus be able to put a better limit on $\Delta\kappa$ than the Tevatron. For λ and $\tilde{\lambda}$, on the other hand, the Tevatron with $\int\mathcal{L}\,dt=100$ pb^{-1} will be able to give a limit which is about a factor 3–5 better than the bound which can be expected from HERA.

Combined, the reactions $p\bar{p}\to W\gamma$ at the Tevatron and $ep\to eWX$ at HERA will yield a precise direct measurement of the $WW\gamma$ vertex before W pair production can be studied at LEP 200. Even in $e^+e^-\to W^+W^-$ at $\sqrt{s}=190$ GeV only an accuracy of $|\Delta\kappa|,|\lambda|,|\tilde{\lambda}|\approx 0.2$ is expected,[37] and in W^+W^- production it is actually a linear combination of $WW\gamma$ and WWZ couplings which will be measured. In view of our present poor knowledge of the values of κ, λ, and $\tilde{\lambda}$, the direct measurement of the $WW\gamma$ couplings via $p\bar{p}\to W\gamma$ at the Tevatron and $ep\to eWX$ at HERA will constitute major progress. In the mid 1990s, these values will also be helpful in disentangling $WW\gamma$ and WWZ anomalous couplings in W pair production at LEP 200.

ACKNOWLEDGMENTS

One of us (U.B.) would like to thank the High Energy Physics Division, Argonne National Laboratory, where this work was initiated, for its warm hospitality. We are grateful to R. Blair, S. Geer, E. W. N. Glover, L. Di Lella, F. Pauss, G. Schuler, J. Smith, C. P. Yuan, and D. Zeppenfeld for stimulating discussions. This research was supported in part by the U.S. Department of Energy, Division of High Energy Physics, Contract No. W-31-109-ENG-38.

*Present address: Physics Department, University of Wisconsin, Madison, WI 53706.

[1]P. Sinervo, in *Proceedings of the XIVth International Symposium on Lepton and Photon Interactions*, Stanford, California, 1989, edited by M. Riordan (World Scientific, Singapore, in press).

[2]R. Johnson, Report No. FERMILAB-Conf-88/169, 1988 (unpublished).

[3]K. O. Mikaelian, Phys. Rev. D **17**, 750 (1978); R. W. Brown, D. Sahdev, and K. O. Mikaelian, *ibid.* **20**, 1164 (1979); K. O. Mikaelian, M. A. Samuel, and D. Sahdev, Phys. Rev. Lett. **43**, 746 (1979); T. R. Grose and K. O. Mikaelian, Phys. Rev. D **23**, 123 (1981).

[4]Zhu Dongpei, Phys. Rev. D **22**, 2266 (1980); C. J. Goebel, F. Halzen, and J. P. Leveille, Phys. Rev. D **23**, 2682 (1981); S. J. Brodsky and R. W. Brown, Phys. Rev. Lett. **49**, 966 (1982); R. W. Brown, K. L. Kowalski, and S. J. Brodsky, Phys. Rev. D **28**, 624 (1983); M. A. Samuel, *ibid.* **27**, 2724 (1983).

[5]C. L. Bilchak, R. W. Brown, and J. D. Stroughair, Phys. Rev. D **29**, 375 (1984).

[6]G. N. Valenzuela and J. Smith, Phys. Rev. D **31**, 2787 (1985).

[7]J. C. Wallet, Z. Phys. C **30**, 575 (1986).

[8]J. Cortes, K. Hagiwara, and F. Herzog, Nucl. Phys. B **278**, 26 (1986).

[9]S.-C. Lee and W. C. Su, Phys. Rev. D **38**, 2305 (1988); Phys. Lett. B **214**, 276 (1988).

[10]K. Hagiwara *et al.*, Nucl. Phys. **B282**, 253 (1987).

[11]U. Baur and D. Zeppenfeld, Nucl. Phys. **B308**, 127 (1988).

[12]J. Smith, D. Thomas, and W. L. van Neerven, Z. Phys. C **44**, 267 (1989).

[13]F. Herzog, Phys. Lett. **148B**, 355 (1984); J. C. Wallet, Phys. Rev. D **32**, 813 (1985); A. Grau and J. A. Grifols, Phys. Lett. B **197**, 437 (1987).

[14]M. Suzuki, Phys. Lett. **153B**, 289 (1985).

[15]J. J. van der Bij, Phys. Rev. D **35**, 1088 (1987).

[16]J. A. Grifols, S. Peris, and J. Solà, Int. J. Mod. Phys. A **3**, 255 (1988).

[17]W. J. Marciano and A. Queijeiro, Phys. Rev. D **33**, 3449 (1986).

[18]F. Hoogeveen, Report No. MPI-PAE/PTh 25/87, 1987 (un-

published).
[19]G. L. Kane, J. Vidal, and C. P. Yuan, Phys. Rev. D **39**, 2617 (1989).
[20]P. Méry, S. E. Moubarik, M. Perottet, and F. M. Renard, Report No. CPT-89/P.2226, 1989 (unpublished).
[21]U. Baur and D. Zeppenfeld, Phys. Lett. B **201**, 383 (1988).
[22]K. Gaemers and G. Gounaris, Z. Phys. C **1**, 259 (1979).
[23]J. M. Cornwall, D. N. Levin, and G. Tiktopoulos, Phys. Rev. Lett. **30**, 1268 (1973); Phys. Rev. D **10**, 1145 (1974); C. H. Llewellyn Smith, Phys. Lett. **46B**, 233 (1973); S. D. Joglekar, Ann. Phys. (N.Y.) **83**, 427 (1974).
[24]T. Kamae, in *Proceedings of the XXIV International Conference on High Energy Physics,* Munich, West Germany, 1988, edited by R. Kotthaus and J. H. Kühn (Springer, Berlin, 1989), p. 156, and references therein.
[25]K. Hagiwara and D. Zeppenfeld, Nucl. Phys. **B274**, 1 (1986).
[26]F. A. Berends *et al.*, Phys. Lett. **103B**, 124 (1981); P. Aurenche *et al.*, *ibid.* **140B**, 87 (1984); Nucl. Phys. **B286**, 553 (1987); V. Barger, T. Han, J. Ohnemus, and D. Zeppenfeld, Phys. Lett. B **232**, 371 (1989).
[27]CDF Collaboration, R. Blair *et al.*, Report No. ANL-HEP-CP-89-07 (unpublished); R. Blair (private communication).
[28]S. A. Kahn *et al.*, BNL informal Report No. 3/83, 1983 (unpublished).
[29]Y. Morita, in *Physics of the Superconducting Super Collider, Snowmass, 1986,* proceedings of the Summer Study, Snowmass, Colorado, 1986, edited by R. Donaldson and J. Marx (Division of Particles and Fields of the APS, New York, 1987), p. 194.
[30]V. Barger, A. D. Martin, and R. J. N. Phillips, Phys. Lett. **125B**, 339 (1983); E. L. Berger, D. DiBitonto, M. Jacob, and W. J. Stirling, *ibid.* **140B**, 259 (1984).
[31]The use of a common K factor for single-vector-boson and vector-boson-pair production has also been conjectured by V. Barger, J. L. Lopez, and W. Putikka, Int. J. Mod. Phys. A **3**, 2181 (1988).
[32]CDF Collaboration, F. Abe *et al.*, Phys. Rev. Lett. **62**, 1005 (1989).
[33]D. Duke and J. Owens, Phys. Rev. D **30**, 49 (1984).
[34]J. Stroughair and C. Bilchak, Z. Phys. C **26**, 415 (1984); J. Gunion, Z. Kunszt, and M. Soldate, Phys. Lett. **163B**, 389 (1985); J. Gunion and M. Soldate, Phys. Rev. D **34**, 826 (1986); W. Stirling *et al.*, Phys. Lett. **163B**, 261 (1985).
[35]L. Di Lella (private communication).
[36]U. Baur and D. Zeppenfeld, Nucl. Phys. **B325**, 253 (1989).
[37]D. Zeppenfeld, Phys. Lett. B **183**, 380 (1987).